

Neural Mechanism of Noise Affecting Face Recognition

Wenlu Li,^{a,b,c} Jin Li,^a Dan Cao,^a Na Luo^a and Tianzi Jiang^{a,b,c,d,e,f,*}

^a Brainnetome Center, Institute of Automation, Chinese Academy of Sciences, Beijing 100190, China

^b National Laboratory of Pattern Recognition, Institute of Automation, Chinese Academy of Sciences, Beijing 100190, China

^c School of Artificial Intelligence, University of Chinese Academy of Sciences, Beijing 100049, China

^d Center for Excellence in Brain Science and Intelligence Technology, Chinese Academy of Sciences, Shanghai 200031, China

^e Key Laboratory for Neuro Information of Ministry of Education, School of Life Science and Technology, University of Electronic Science and Technology of China, Chengdu 610054, China

^f Queensland Brain Institute, University of Queensland, 4072 Brisbane, Australia

Abstract—Face recognition is one of the most important cognitive functions for humans in social activities. The ability will be negatively affected when the face images deteriorate. However, the neural process of extracting facial information under challenging conditions is still poorly understood. Therefore, it is necessary to further understand the neurophysiological relevance of this effect. We examined patients with multiple subdural electrodes (ECoG) monitored for clinical purposes. During the experimental task, the patients were presented with face and house images with different noise levels and were asked to recognize the faces. We found a striking increase in high gamma band power (HGP; 60–160 Hz) when face images were shown. We localized the face-specific electrodes to the fusiform gyrus (FG) and surrounding cortices. For each subject, the behavioral performance and magnitudes of the HGP for the face-specific sites significantly both fit a sigmoid function and showed similar changes. Additionally, the curve profile of the average HGP magnitude across the face-specific sites was almost equal to the average behavior curve; the former could precisely track the behavioral performance. In general, these results suggest that the HGP in the FG is closely related to the performance of face image recognition. © 2021 IBRO. Published by Elsevier Ltd. All rights reserved.

Key words: high gamma power, sigmoid, fusiform gyrus, ECoG.

INTRODUCTION

Face recognition is one of the most important cognitive functions of human beings. Accurate recognition of faces is essential for social interaction. It seems to have a natural sensitivity to human faces and can easily classify visual stimuli as faces in various situations. Previous research has made significant progress in identifying the neural basis of humans' efficient and effortless facial perception. But in real life, we are faced with problems such as loss of eyesight or deterioration of facial images, so that the face we see may be blurred, which negatively affects our face recognition ability. However, we still know very little about the neural process of how to extract facial information under challenging conditions. It is therefore necessary to

investigate what happens to the human brain when it processes face images with added noisy information.

For the past three decades, external noise has been added to visual stimuli to study visual processing in the fields of visual psychophysics and face perception by utilizing electrophysiology and brain imaging (Costen et al., 1994; Gold et al., 1999). Research studies related to face image noise have primarily focused on face-sensitive event-related potential (ERP) components obtained by electroencephalography (EEG). These showed that, with increases in the level of face image noise, the absolute value of the amplitude of the N170 component (the negative component that peaked about 170 ms after stimulation onset) decreased linearly while the P1 component (the positive component that peaked about 100 ms after stimulation onset) was stable (Jemel et al., 2003) and that the later P2 component (the positive component that peaked about 200 ms after stimulation onset) was enhanced (Philiastides et al., 2006). In brief, increases in face noise level are usually considered to lead to changes in the face-sensitive ERP.

*Correspondence to: T. Jiang, Brainnetome Center, Institute of Automation, Chinese Academy of Sciences, Beijing 100190, China. E-mail address: jiangtz@nlpr.ia.ac.cn (T. Jiang).

Abbreviations: ECoG, electrocorticography; EEG, electroencephalography; ERP, event-related potential; FG, fusiform gyrus; HGP, high gamma band power.

However, it is difficult for ERP to express information derived from induced activity, which mainly reflects high-cognitive rather than perceptual activity and can be retrieved by time–frequency analyses (Donner and Siegel, 2011). Previous studies using subdural electrophysiological recordings have indicated that high-order, face-specific electrodes show a face recognition-related effect at high frequency (mainly in the broadband gamma band 30–150 Hz) (Tsuchiya et al., 2008; Fisch et al., 2009; Engell and McCarthy, 2011; Aru et al., 2012). The induced gamma band oscillation may be a sign of holistic face processing supported by evidence that upright face perception, as compared to inverted face or object perception, is mediated by stronger gamma-band activity (Bossi et al., 2020). Moreover, it has been suggested that gamma band activity reflects the synchronization of oscillatory neuronal assemblies thought to underlie the formation of cortical object representations (Engel and Singer, 2001; Donner and Siegel, 2011) and may be related to perception (Rodriguez et al., 1999) and structural encoding of faces (Zion-Golumbic and Bentin, 2007; Gao et al., 2013). In addition, such face-specific electrodes were mainly in face-selective regions, which consisted of the fusiform gyrus (FG) and surrounding areas of the human ventral temporal cortex and which were identified based on stronger responses to faces than to a variety of other stimuli (Grill-Spector et al., 2017). Intracranial EEG places electrodes directly within targeted neuronal populations to collect the electrical signals of specific brain regions and allows the investigation of face processing by providing precise information about the temporal structure of neuronal responses. Interestingly, the perceptual ability of humans to identify face images in the presence of noise varies nonlinearly as a function of how much noise is introduced to the stimuli. Specifically, the accuracy holds at a high level in the low noise range and declines rapidly in the medium noise range (Costen et al., 1994; Perry, 2016). Although previous studies found that the ERP components decreased with increasing noise, relatively little is known about the link between the neural signal and perceptual abilities in the presence of noise.

In this research, we used intracranial EEG recordings (ECoG) to study how the signals in the human ventral temporal cortex, especially the FG, change in the gamma band when watching a series of face images with different noise levels and how they correlate with human behavior.

EXPERIMENTAL PROCEDURES

Human subjects

We studied four subjects (2 men and 2 women) who were epileptic patients at Harborview Hospital in Seattle, Washington. Subdural grid and platinum arrays (4 mm diameter, 2.3 mm exposed, and 10 mm interelectrode distances; Ad-Tech, Racine, WI) were placed in the occipitotemporal cortex for clinical monitoring and localization of epileptic foci. The basic information about each subject (gender, age, handedness, and grid location) is shown in Table 1. Before testing, all the subjects provided written informed consent for the

study, which was approved by the Institutional Review Board of the University of Washington (no. 12193). Behavioral parameters, electrode positions, and electrophysiological signals were recorded and shared in a freely available library at <https://searchworks.stanford.edu/view/zk881ps0522> created by Kai J. Miller et.al (Miller et al., 2017; Miller, 2019).

Electrode localization

The electrode positions and the brain regions they belong to are described in the database. The electrode positions were located on structural MRI images using postimplant computed tomography (CT), utilizing the CTMR package and FreeSurfer-rendered cortical reconstructions (Dale et al., 1999; Hermes et al., 2010). For simplicity, the word “site” was used to represent the electrode contact. Most sites were located in the inferotemporal gyrus, which includes the following gyri: temporal pole, parahippocampal gyrus, inferior temporal gyrus, middle temporal gyrus, FG, lingual gyrus, and inferior occipital gyrus (Destrieux et al., 2010). The details of the sites for each subject are shown in Fig. 1B and Table 2.

Experimental design

The details of the experimental paradigm were described by Miller et al. (2017). In brief, all four subjects completed two experiments, a basic task and a noisy task. In the basic task, the subjects watched grayscale pictures of faces and houses, which were displayed in random order, one picture in a trial, for 400 milliseconds with a 400 milliseconds blank screen inter-stimulus interval (ISI; Fig. 1A). A total of 300 stimuli were shown to each subject, 100 stimuli for each run. Stimuli were balanced for the number of face and house pictures.

In the noisy task, the subjects were asked to perform a face-recognition task using phase-scrambled images of faces and houses. These stimuli images all had an identical frequency power spectrum but with graded amounts of phase noise (ranging from 0 to 100% noise, in 5% increments). Each image was shown for 1000 ms with no ISI. The subjects were instructed to press button the “F” key if they believed the picture to be that of a face. A total of 630 stimuli were shown to each subject, 105 stimuli for each run. The stimuli were randomly interleaved and balanced for noise level and number of face and house images (Fig. 1A).

Statistical analyses

The significant differences between experimental conditions (face images vs. house images) were determined by a non-parametric cluster-based permutation test (Maris and Oostenveld, 2007). Cluster-level statistics were computed by taking the sum of the *t* values within a cluster. The distribution of cluster-level statistics under the null hypothesis was constructed by randomly permuting condition labels for 1000 times, and the maximum cluster-level statistic in each permutation was extracted. The nonparametric statistical significance was obtained by calculating the proportion of surrogates

Table 1. Basic information for each subject. The gender, age, handedness, and grid location

Subject	Gender	Age	Handedness	Grid Location
S1	F	27	Right	L Fronto-temporal-parietal
S2	M	32	Right	L Fronto-temporal-parietal
S3	F	45	Right	L Frontotemporal
S4	M	37	Unknown	Subtemporal / Occipital

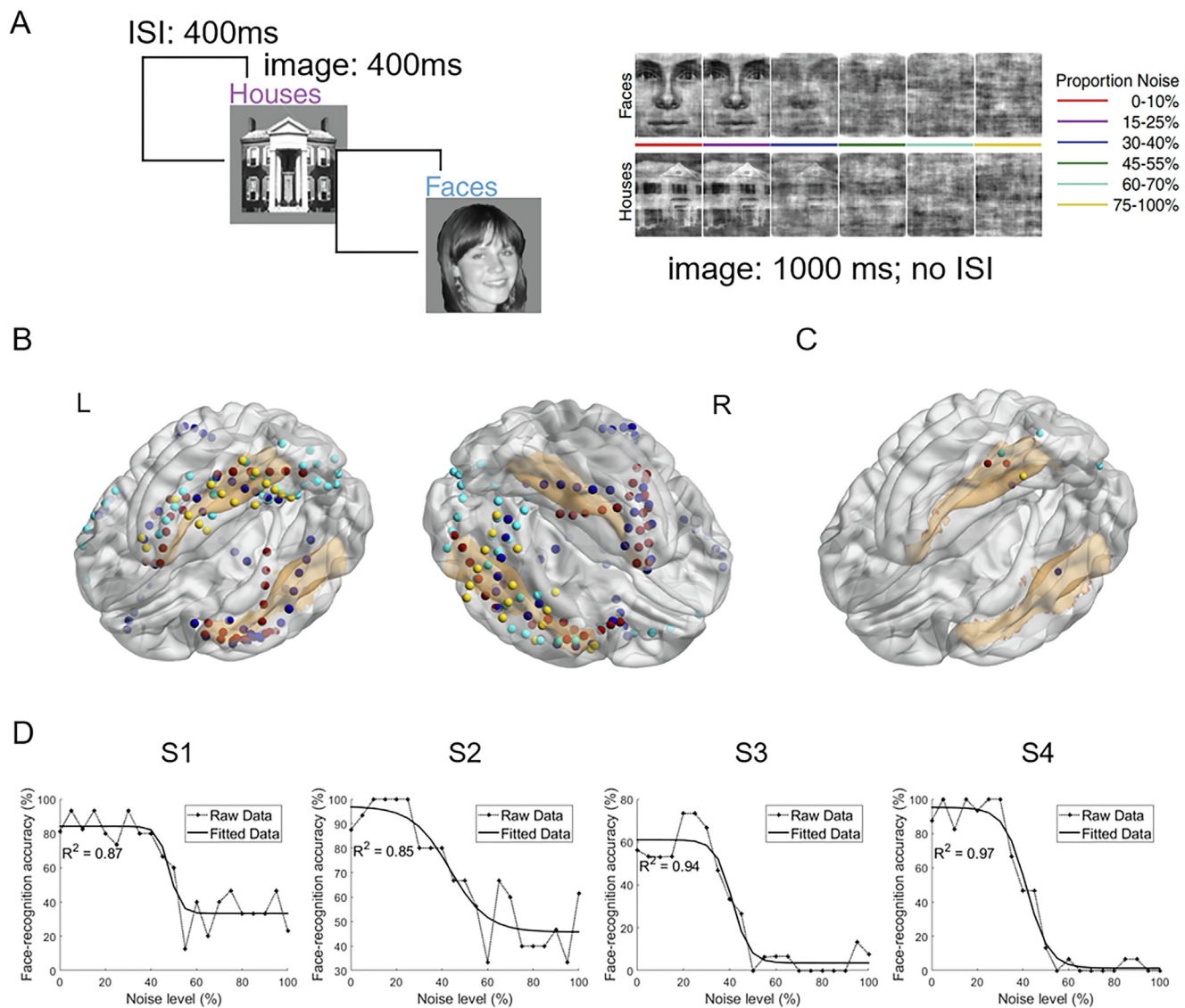


Fig. 1. Face-recognition experiment, electrode localization and task performance. **(A)** Left panel: Basic task, grayscale pictures of faces and houses were shown in random order for 400 ms each with a 400 ms ISI of blank screen. Right panel: Noisy task, for each noise level (ranging from 0 to 100% noise in 5% increments), phase-scrambled pictures of faces and houses were displayed in random order for 1 s each with no ISI; the subjects were required to press a key when they believed that the picture showed a face. Adapted from Miller et al. (2017). **(B)** Electrode positions in all 4 subjects are displayed on ventral left and right view of a MNI cortex. Orange shadow represents the FG. Each dot presents a site, and the sites of different subjects are distinguished by different colors (S1: dark blue; S2: light blue; S3: yellow; S4: red). Most of the sites were located in the inferotemporal gyrus. **(C)** Electrode positions of the face-specific sites, which were determined by contrasting the responses to face images with those to house images. **(D)** Plots of face recognition accuracy for varying noise levels in each of the four subjects. Black cross symbol represents the actual data. Black line shows the best fitting sigmoid function (R^2 for each fit is given in each plot). (For interpretation of the references to colour in this figure legend, the reader is referred to the web version of this article.)

within the permutation distribution that exceeded the observed cluster-level statistics (e.g., $p = 0.05$ observed data exceed 95% surrogate data). Nonlinear regression

was used to fit the observed behavioral and electrophysiological data, and a χ^2 square goodness-of-fit test was carried out to test the degree and significance of the fit

Table 2. Details of the sites for each subject. Number of cortical sites and FG sites after rejecting sites with significant artifacts. Region and response properties of the face-specific sites. Each row represents a face-specific site

Subject	Number of cortical sites	Number of FG sites	Region of face-specific sites	Fit of sigmoidal (R^2)
S1	58	5	FG	0.86
			FG	0.65
S2	37	5	FG	0.48
			Lingual	0.48
			MOG	0.91
S3	53	2	FG	0.69
S4	40	2	FG	0.77
			FG	0.97

FG: fusiform gyrus; MOG: middle occipital gyrus; Lingual: lingual gyrus.

between the original data and the function. The relationship between the gamma band power and face recognition accuracy was analyzed using a Spearman correlation test. The stronger the correlation between the two variables, the greater the absolute value of Spearman coefficient. All data analysis was conducted using Matlab (The MathWorks, Inc., Natick, Massachusetts).

ECoG data analysis

Preprocessing. Electrical potentials were sampled at 1000 Hz with an instrument-imposed bandpass filter from 0.15 to 200 Hz. In the basic task, we first filtered the data for line noise (between 58 and 62 Hz) and harmonics (118–122 Hz and 178–182 Hz) using 3rd-order Butterworth band-stop filters. The sites underwent an automatic quality assessment to reject artifacts: sites with signal variances five times larger or smaller than the average variance across the sites were considered as pathological. Sites with three times more “jumps” (defined as changes in the signal derivative $> 100 \mu\text{V}$) than the average across the sites were labeled as spiky. All pathological and spiky sites were excluded from further analysis. Then the electrical potentials were re-referenced to the average of the signal over all the selected sites. Each epoch was extracted in the $[-200 \text{ } 600]$ ms time window around the stimulus onset, and a baseline correction was performed in the $[-200 \text{ } -50]$ ms time window around the stimulus onset. Prior to the time–frequency analysis, we removed the signal-averaged ERP from the raw potential signal for each trial. This ensured that any significant spectral differences did not merely reflect the frequency composition of the phase-locked ERP.

Frequency bands specifically activated by face images. A time–frequency decomposition was then computed using a seven-cycle Morlet wavelet, with frequencies ranging from 1 to 200 Hz (1 Hz steps). The power values in each frequency bin were log transformed and normalized using the max of the log-transformed power values. For each frequency, the power values $[50 \text{ } 300]$ ms after stimulation were summed, and then the two-dimensional signals of frequency and power were obtained. Paired non-parametric permutation tests (10,000 permutations) were used on the two-dimensional signals to assess

which frequency band was significantly activated ($p < .05$) by the face images compared with the house images. This was calculated for each site.

Power induced in the specific active frequency band by face images at different noise levels. The preprocessing steps for the noisy task were the same as those for the basic task. After the data were notch filtered and re-referenced to the average signal over all the selected sites, each epoch was extracted in the $[0 \text{ } 1000]$ ms post-stimulus time window. Then the electrophysiological signal was decomposed (1 Hz steps) in the frequency band specifically activated by the face images. The signal was finally averaged across the face-specific frequency and smoothed with a 50 ms width Gaussian window. To verify that this response was stable across the trials and was not caused by an abnormal discharge in one of the trials, we also generated the representation of the power \times time data for all the individual face image trials and arranged these trials in rows according to the noise levels.

Face-specific sites

In order to obtain stable face-specific sites, a site was defined as “face-specific” if the magnitude of power in the specific active frequency band for face images was significantly greater than that caused by house images in both basic and noisy task. During the selection of trials in noisy task in analyzing “face-specific” sites, there is a trade-off between the power benefits from including more trials and the risk of including non-face-processing components in trials with high noisy level. Finally, we used images in the noise range of 0–30%, in which the face recognition ability remained high without a sharp reduction of performance (Fig. 1D). A permutation test assessed the significant difference between the magnitude of power for face images and that caused by house images of the response at $p < .05$.

Fitting function

Based on the shape of the data varying with noise level, a nonlinear regression was used to fit the recognition accuracy and electrophysiological signals. The sigmoid function for fitting was defined as the following function

$$f(x) = \frac{a_1}{1 + e^{-a_2(x+a_3)}} + a_4$$

where a_i represents free parameters, and $-a_3$ was the noise level for which the sigmoid curve reached its inflexion point. The threshold range that describes the stage where the curve declined rapidly was defined as $[-a_3 - 10, -a_3 + 10]$.

RESULTS

Behavior performance

For each subject, we calculated the recognition accuracy for each noise level and found that, with a change of noise, the accuracy follows an S-shaped curve. That is, at a low noise level (from about 0 to 30%), the recognition accuracy stayed high; at a high noise level (from about 60 to 100%), the recognition accuracy was low; and at a middle noise level (from about 35 to

55%), the recognition accuracy showed an abrupt change to bridge the difference.

Then, we found that for each subject the curve relating the recognition accuracy to noise levels of face images well fit the sigmoid function (S1: $R^2 = 0.87$; S2: $R^2 = 0.85$; S3: $R^2 = 0.94$; S4: $R^2 = 0.97$, χ^2 square goodness-of-fit test) (Fig. 1D).

Power induced by face images in basic and noisy task

In the basic task, for each subject, there were such sites that the power in the frequency range of about [60 160] Hz was significantly induced by face images (S1: [54 165] Hz, $p = 10^{-4}$; S2: [78 167] Hz, $p = 3 \times 10^{-4}$; S3: [52 168] Hz, $p = .0012$; S4: [80 160] Hz, $p = 7 \times 10^{-4}$) (Fig. 2A). Therefore, the power induced by the noisy

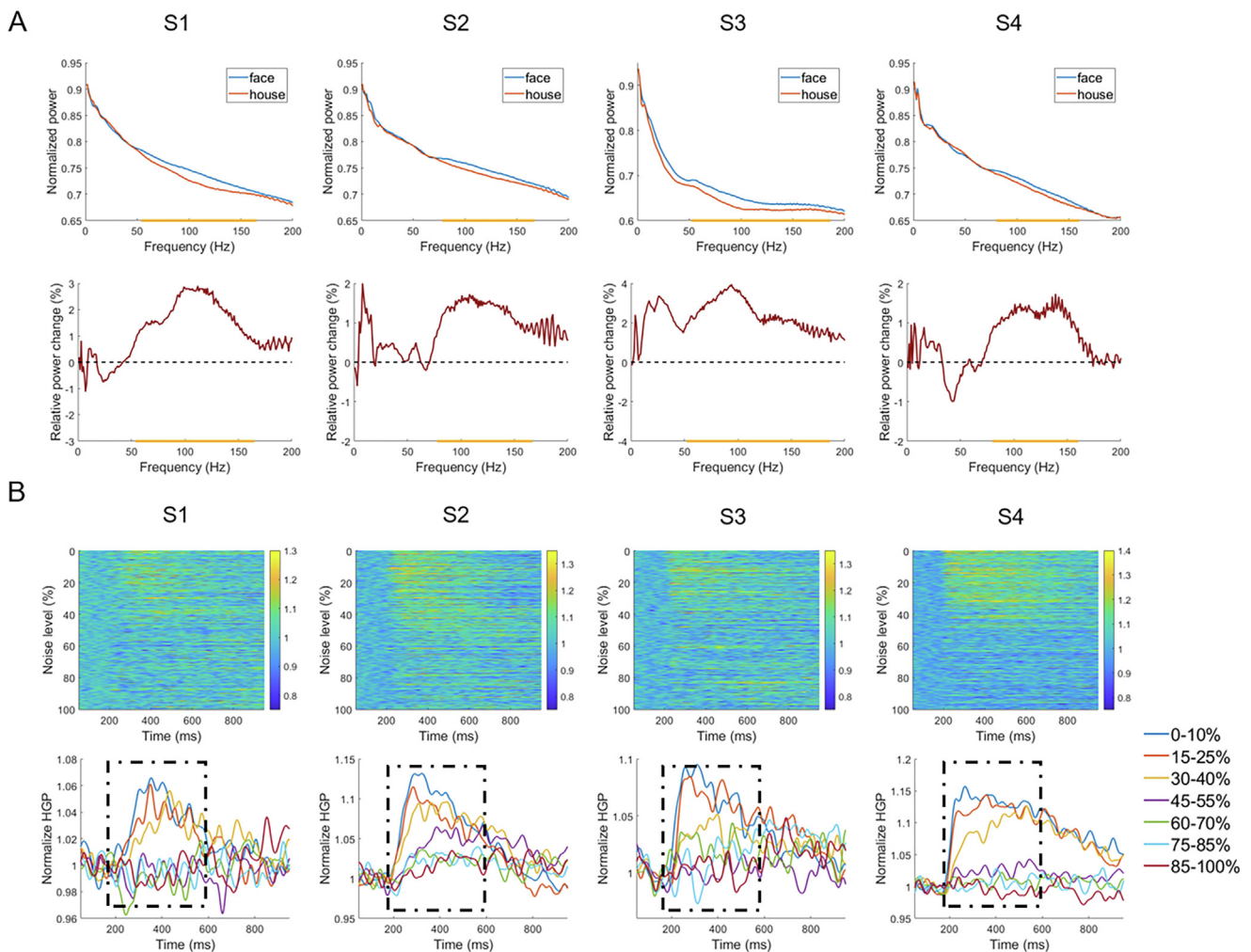


Fig. 2. The specific frequency band for the individual sites activated by face images and under different face noise levels. **(A)** Upper panel: Power-spectrum change in response to face images and house images along the whole frequency band of the individual site for each subject in the basic task. The difference was significant at the $p < .05$ level in a broad range of high gamma frequencies ranging from about 60 to 160 Hz, as indicated by the yellow line. Lower panel: Relative power-spectrum change between face vs. house images of the individual site. **(B)** Upper panel: Time course of the high gamma band power (HGP; 60–160 Hz) in the face image trials in the noisy task is displayed from top to bottom in the order of increasing noise levels. Warmer colors indicate higher activation. Most of the trials at low noise levels had high activations. Lower panel: Time course of average HGP for different noise levels of face image trials in the noisy task. The [200 600] ms post-stimulus time window captured the greatest changes in the HGP, as indicated by the black dotted rectangles. (For interpretation of the references to colour in this figure legend, the reader is referred to the web version of this article.)

face image was calculated in this high gamma frequency band. The power in the frequency band at the low noise level was more strongly activated than that of the high noise level, and this response was stable across trials (Fig. 2B, upper panel). After inspecting the time course of the high gamma power (HGP) for different noise levels of face images, the magnitude of the HGP was calculated as the area under the curve (AUC) in the [200 600] ms post-stimulus window, which captured the largest changes in the HGP (Fig. 2B, lower panel). In the end, we identified eight face-specific sites across the subjects, six of which were located in the FG, and all four subjects had face-specific sites in the FG (Fig. 1C; Table 2).

Magnitudes of the HGP for face-specific sites in the face-recognition task

We examined the face-specific sites for each subject to see how the magnitudes of the HGP were induced by varying the noise level of the face images. We found that they all decreased and exhibited a nonlinear signature with increasing noise level, similar to the nonlinear response in the behavioral data. The observations were confirmed statistically by fitting the magnitudes using the sigmoid fitting function, and each subject's electrophysiological data were fit with the function ($S1 : R^2 = 0.88$; $S2 : R^2 = 0.84$; $S3 : R^2 = 0.69$; $S4 : R^2 = 0.95$, χ^2 goodness-of-fit test). In addition, the threshold range for the magnitudes of the HGP for each subject accuracy was close to that of recognition accuracy (from about 35–55%). To rule out the possibility that the curve profile was caused by the visual noise rather than by a sensory response to the face images, the data for these face-specific sites, but obtained using the house images, was fit to a sigmoidal curve. In contrast to the facial data, none of

the house data showed a significant fit to the sigmoid curve

($S1 : R^2 = 0.03 = 0.16$; $S3 : R^2 = 0.07$; $S4 : R^2 = 0.22$, χ^2 square goodness-of-fit test) (Fig. 3).

Correlation between recognition accuracy and HGP

A Spearman correlation analysis was used to analyze the relationship between the face recognition accuracy and the HGP induced by the face images. The result showed that the magnitudes of the HGP for the face-specific sites were significantly positively correlated with the recognition accuracy of each subject ($S1 : r = 0.77$, $p = 3.8 \times 10^{-5}$; $S2 : r = 0.76$, $p = 7.0 \times 10^{-5}$; $S3 : r = 0.68$, $p = 6.8 \times 10^{-4}$; $S4 : r = 0.83$, $p = 3.6 \times 10^{-6}$, Spearman correlation) (Fig. 4A).

At the group level, we pooled the face-specific sites across the subjects to generate the average magnitudes of the HGP for the face images and pooled the recognition accuracy across the subjects to generate the average recognition accuracy. The sigmoid function was then used to fit both the average magnitudes of the HGP and the average recognition accuracy at varying noise levels. It turns out that both the neural signals and the behavioral data were significantly correlated with the sigmoid function (magnitudes : $R^2 = 0.96$; recognition accuracy : $R^2 = 0.98$, χ^2 square goodness-of-fit test). In addition, the threshold range for the magnitudes of the HGP was almost equal to that of recognition accuracy (32–52% vs. 33–53%) (Fig. 4B).

DISCUSSION

In this paper, we studied how the high gamma signal in FG and its adjacent cortex changes with different noise levels in face images and its relationship with human face recognition accuracy. First, we found a striking increase in the high gamma frequency band (60–

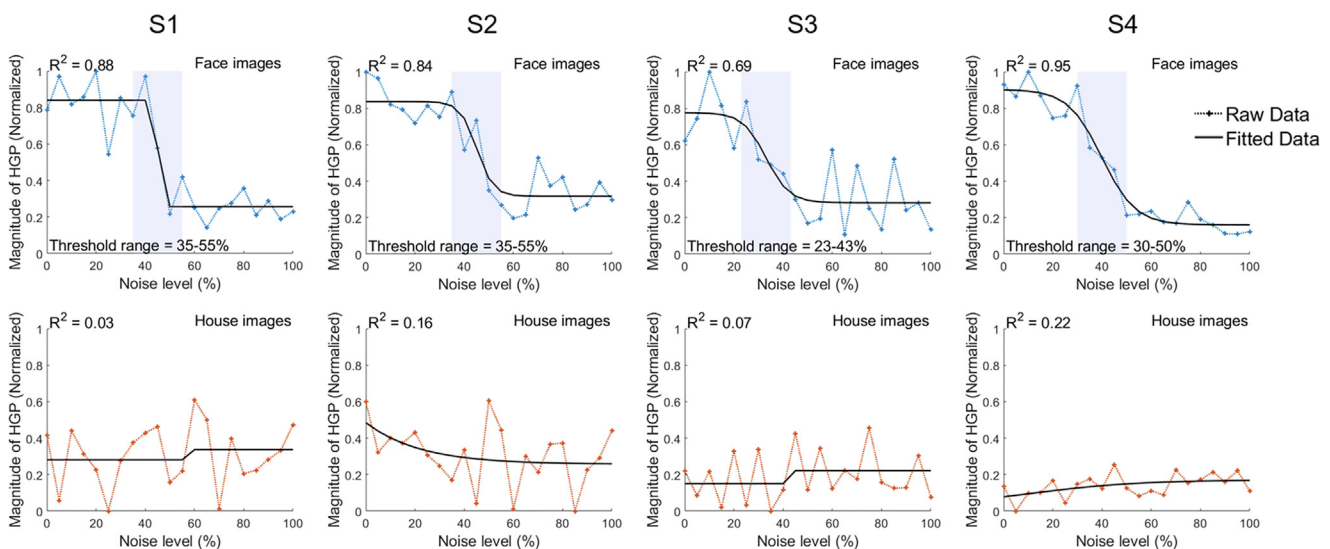


Fig. 3. Magnitudes of the HGP for varying noise levels at face-specific sites. The normalized magnitudes of the HGP of the face images (upper panel) and house images (lower panel) using the sigmoid fitting function. Colored cross symbol represents the actual data. Black line shows the best fitting sigmoid function (R^2 for each fit is given in plot), and the shadows show the threshold range. (For interpretation of the references to colour in this figure legend, the reader is referred to the web version of this article.)

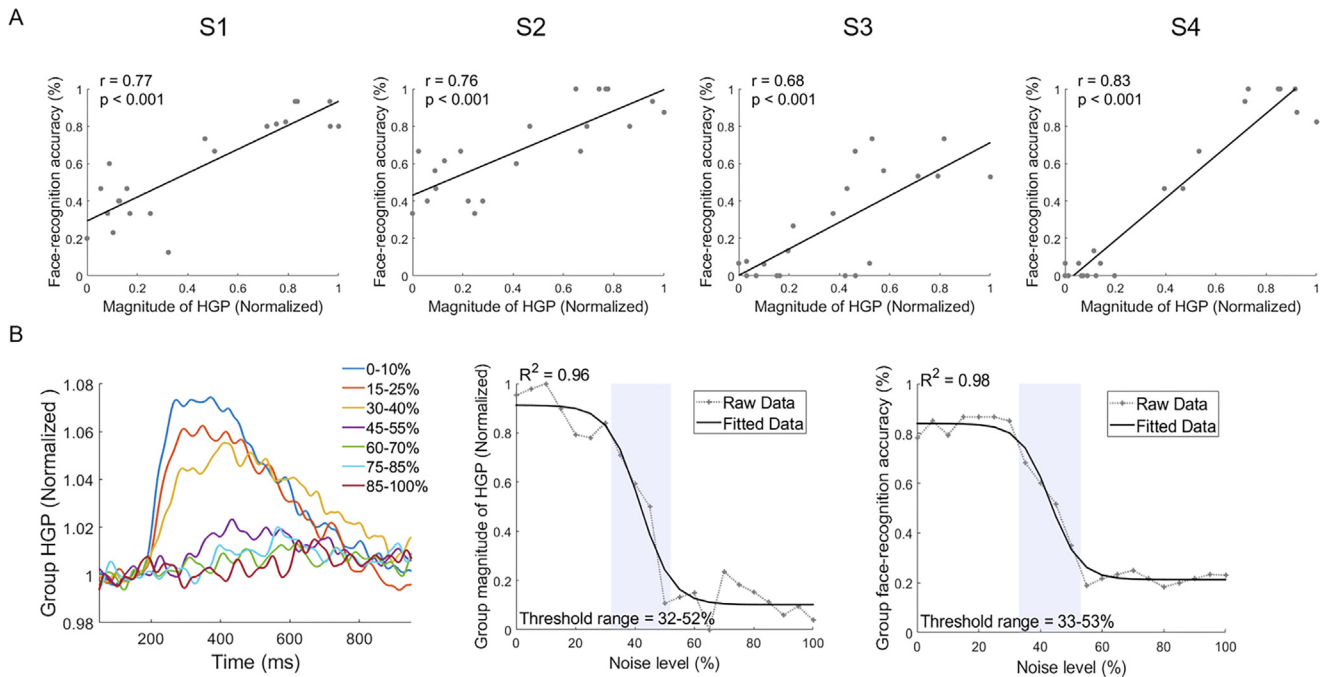


Fig. 4. Relationship between recognition accuracy and the HGP of the face-specific sites. **(A)** Spearman correlation between recognition accuracy and magnitudes of the HGP of face-specific sites for each subject. Each dot represents a noise level (correlation coefficient r and significance p value are given in each plot). **(B)** Left panel: Time course of the average HGP for different noise levels of face images across the face-specific sites for all subjects. Middle panel: Average magnitudes of the HGP induced by face images across face-specific sites for all subjects. Right panel: Average recognition accuracy of the face images across all subjects. For the middle and the right panel, the sigmoid fitting function was used to fit the magnitudes. Black cross symbol represents the actual data. Black line shows the best fitting sigmoid function (R^2 for each fit is given in plot), and the shadows show the threshold range.

160 Hz) when face images were shown, and eight face-specific sites were identified based on the HGP, including six in the FG. Second, our results demonstrated that, for the face-specific sites, the curve of the magnitudes of the HGP induced by the varying noise levels of the face images had a profile similar to that of face recognition accuracy, both showing S-shaped curves. Correlation analyses indicated that the magnitudes of the HGP induced by face images were significantly correlated with the subject's performance in the face recognition task. Finally, at the group level, we found that the curve profile of the average magnitudes of HGP across the face-specific sites was almost the same as the average recognition accuracy curve. In general, these results suggest that the HGP in the FG is closely related to the accuracy in the face recognition task. These findings promote our understanding of the neural mechanism of how noise affects face recognition.

A previous study using phase-scrambled pictures of face images showed that for the 25 participants in that study the plots of the psychometric functions of face detection under varying levels of phase noise all fit an S-shaped curve well, a finding which is consistent with the behavioral performance of the four subjects in our study (Perry, 2016). There is no doubt that people often have greater difficulty recognizing face images with a high noise level than those with a low noise level, but the recognition accuracy does not change linearly with a linear change in image ambiguity. One of the basic characteristics of human perception is that small changes in

stimuli can induce changes in perceptual states, leading to the sigmoidal shape of the psychometric curve (Green and Swets, 1974), however, the neural mechanism behind this behavior pattern has been unclear. Here we found that in specific brain regions, signals in the high gamma frequency band showed a change that had a similar profile to that of behavioral performance.

Cortical oscillatory synchrony in the gamma band (> 30 Hz) has attracted increasing attention in cognitive neuroscience in the past several decades because of suggestions that gamma band activity represents complex cognitive mechanisms. Gamma oscillations (30–150 Hz) induced during face perception along the human ventral occipitotemporal cortex (mainly in the FG) have been discovered in previous studies using implanted electrodes (Tsuchiya et al., 2008; Engell and McCarthy, 2011; Aru et al., 2012). Recent MEG research found that during stimulus processing, the gamma-band oscillations of extra-striate (fusiform/lingual gyrus) cortices in schizophrenia patients were prominently impaired, while the baseline spectrum were intact. Importantly, the impairment in oscillatory activity correlated with reduced behavioral detection rates (Grent-t-Jong et al., 2016, 2018). Our finding is in line with these studies, and they together suggest the association between gamma-band oscillations and behavioral performance. Additionally, the human FG can be further parcellated into three functionally distinct parts, the medial portion (FGm), the lateral portion (FGl), and the anterior portion (FGa), using diffusion tensor imaging, according to the Brainnetome atlas

(Fan et al., 2016; Zhang et al., 2016). To locate the face-specific sites on a more accurate scale, we registered the FG of the Brainnetome atlas to the individual T1 MRI images to discover the subregion in which the face-specific electrodes were located. Interestingly, out of the six FG face-specific sites, four of them were located in FGI, which is responsible for categorical recognition. The location distribution of face-specific sites supports our conclusion as well.

A study based on fMRI found that when subjects were presented with face images and object images with different contrasts, the sensitivity of the fMRI signal to the contrast gradually decreased along the lateral occipital cortex from the primary visual cortex to the high order cortex. Although the posterior FG showed greater sensitivity to changes in the contrast in the object images, it was less sensitive to changes in the contrast in the face images, indicating that the activation of face images in the FG was caused by facial features rather than visual clarity (Avidan et al., 2002). On the other hand, Engell and McCarthy (2011) compared the response of induced gamma oscillations between 30 and 100 Hz in the ventral occipitotemporal gyrus to simple faces, complex faces, and greebles (nonface control stimulus, similar to faces along several dimensions). His results suggested that the higher induced gamma signal in response to complex stimuli might support high-order processing rather than an obligatory response to simple face features in that the signal induced by simple faces did not differ from the greeble stimuli and that both were significantly smaller than the signal induced by complex faces. We speculate that the amount of high-order information in face images extracted by the high gamma signal of the FG remains unchanged in the low noise range (about 0–30%), therefore, the magnitude of the HGP in the FG remained unchanged within the low noise range.

Our results confirmed that there was a correlation between the HGP in the FG and the face-recognition performance in four subjects. This finding occurred in each subject. This result also raised the possibility that disrupting the high gamma activity in the FG may reduce the accuracy in face recognition tasks. Future studies using invasive techniques can be used to test these hypotheses in further studies to understand the causal relationship between them.

ACKNOWLEDGMENTS

We thank Rhoda Perozzi for her language help in the process of writing the paper. This work was supported by the Natural Science Foundation of China [grant numbers 91432302, 31620103905]; the Science Frontier Program of the Chinese Academy of Sciences [grant number QYZDJ-SSW-SMC019]; the China Postdoctoral Science Foundation [grant number BX20200364]; and the Guangdong Pearl River Talents Plan [grant number, 2016ZT06S220].

REFERENCES

Aru J, Axmacher N, Do Lam AT, Fell J, Elger CE, Singer W, Melloni L (2012) Local category-specific gamma band responses in the

- visual cortex do not reflect conscious perception. *J Neurosci* 32:14909–14914.
- Avidan G, Harel M, Hendler T, Ben-Bashat D, Zohary E, Malach R (2002) Contrast sensitivity in human visual areas and its relationship to object recognition. *J Neurophysiol* 87:3102–3116.
- Bossi F, Premoli I, Pizzamiglio S, Balaban S, Ricciardelli P, Rivolta D (2020) Theta- and gamma-band activity discriminates face, body and object perception. *Front Hum Neurosci* 14:74.
- Costen NP, Parker DM, Craw IJP (1994) Spatial content and spatial quantisation effects in face recognition. *Perception* 23:129–146.
- Dale AM, Fischl B, Sereno MI (1999) Cortical surface-based analysis. I. Segmentation and surface reconstruction. *Neuroimage* 9:179–194.
- Destrieux C, Fischl B, Dale A, Halgren E (2010) Automatic parcellation of human cortical gyri and sulci using standard anatomical nomenclature. *Neuroimage* 53:1–15.
- Donner TH, Siegel M (2011) A framework for local cortical oscillation patterns. *Trends Cogn Sci* 15:191–199.
- Engel AK, Singer W (2001) Temporal binding and the neural correlates of sensory awareness. *Trends Cogn Sci* 5:16–25.
- Engell AD, McCarthy G (2011) The relationship of gamma oscillations and face-specific ERPs recorded subdurally from occipitotemporal cortex. *Cereb Cortex* 21:1213–1221.
- Fan L, Li H, Zhuo J, Zhang Y, Wang J, Chen L, Yang Z, Chu C, et al. (2016) The human brainnetome atlas: a new brain atlas based on connective architecture. *Cereb Cortex* 26:3508–3526.
- Fisch L, Privman E, Ramot M, Harel M, Nir Y, Kipervasser S, Andelman F, Neufeld MY, et al. (2009) Neural “ignition”: enhanced activation linked to perceptual awareness in human ventral stream visual cortex. *Neuron* 64:562–574.
- Gao Z, Goldstein A, Harpaz Y, Hansel M, Zion-Golumbic E, Bentin S (2013) A magnetoencephalographic study of face processing: M170, gamma-band oscillations and source localization. *Hum Brain Mapp* 34:1783–1795.
- Gold J, Bennett PJ, Sekuler AB (1999) Signal but not noise changes with perceptual learning. *Nature* 402:176–178.
- Green DM, Swets JA (1974) Signal detection theory and psychophysics. Huntington, N.Y.: R. E. Krieger Pub. Co.
- Grent-t-Jong T, Rivolta D, Gross J, Gajwani R, Lawrie SM, Schwannauer M, Heidegger T, Wibrat M, et al. (2018) Acute ketamine dysregulates task-related gamma-band oscillations in thalamo-cortical circuits in schizophrenia. *Brain* 141:2511–2526.
- Grent-t-Jong T, Rivolta D, Sauer A, Grube M, Singer W, Wibrat M, Uhlhaas PJ (2016) MEG-measured visually induced gamma-band oscillations in chronic schizophrenia: Evidence for impaired generation of rhythmic activity in ventral stream regions. *Schizophr Res* 176:177–185.
- Grill-Spector K, Weiner KS, Kay K, Gomez J (2017) The functional neuroanatomy of human face perception. *Annu Rev Vision Sci* 3 (3):167–196.
- Hermes D, Miller KJ, Noordmans HJ, Vansteensel MJ, Ramsey NF (2010) Automated electrocorticographic electrode localization on individually rendered brain surfaces. *J Neurosci Methods* 185:293–298.
- Jemel B, Schuller AM, Cheref-Khan Y, Goffaux V, Crommelinck M, Bruyer R (2003) Stepwise emergence of the face-sensitive N170 event-related potential component. *Neuroreport* 14:2035–2039.
- Maris E, Oostenveld R (2007) Nonparametric statistical testing of EEG- and MEG-data. *J Neurosci Methods* 164:177–190.
- Miller KJ (2019) A library of human electrocorticographic data and analyses. *Nat Hum Behav* 3:1225–1235.
- Miller KJ, Hermes D, Pestilli F, Wig GS, Ojemann JG (2017) Face percept formation in human ventral temporal cortex. *J Neurophysiol* 118:2614–2627.
- Perry G (2016) The visual gamma response to faces reflects the presence of sensory evidence and not awareness of the stimulus. *R Soc Open Sci* 3 150593.
- Philastides MG, Ratcliff R, Sajda P (2006) Neural representation of task difficulty and decision making during perceptual categorization: A timing diagram. *J Neurosci* 26:8965–8975.

- Rodriguez E, George N, Lachaux JP, Martinerie J, Renault B, Varela FJ (1999) Perception's shadow: long-distance synchronization of human brain activity. *Nature* 397:430–433.
- Tsuchiya N, Kawasaki H, Oya H, Howard 3rd MA, Adolphs R (2008) Decoding face information in time, frequency and space from direct intracranial recordings of the human brain. *PLoS One* 3 e3892.
- Zhang W, Wang J, Fan L, Zhang Y, Fox PT, Eickhoff SB, Yu C, Jiang T (2016) Functional organization of the fusiform gyrus revealed with connectivity profiles. *Hum Brain Mapp* 37:3003–3016.
- Zion-Golumbic E, Bentin S (2007) Dissociated neural mechanisms for face detection and configural encoding: evidence from N170 and induced gamma-band oscillation effects. *Cereb Cortex* 17:1741–1749.

(Received 9 March 2021, Accepted 11 June 2021)
(Available online 18 June 2021)